Semiconductor Physics, Quantum Electronics & Optoelectronics, 2022. V. 25, No 3. P. 294-302.

Semiconductor physics

Grain size effect on electrical properties of Ag_6PS_5I-based ceramic materials

A.I. Pogodin[1*], I.O. Shender[1], M.J. Filep[1,2], O.P. Kokhan[1], O.I. Symkanych[1], T.O. Malakhovska[1], L.M. Suslikov[1], P. Kopčanský[3]

[1]*Uzhhorod National University, 46, Pidgirna str., 88000 Uzhhorod, Ukraine*
[2]*Ferenc Rákóczi II Transcarpathian Hungarian Institute, 6, Kossuth Sq., 90200 Beregovo, Ukraine*
[3]*Institute of Experimental Physics, Slovak Academy of Sciences, 47, Watsonova str., 04001 Košice, Slovakia*
**Corresponding author e-mail: artempogodin88@gmail.com*

Abstract. Micro- and nanocrystalline powders were prepared by grinding of pre-synthesized Ag_6PS_5I in an agate mortar and a planetary ball mill, which were further investigated using XRD and SEM methods. Appropriate ceramic materials in the form of disks with a relative density of (91…94) ± 1% of the theoretical one were made using the cold pressing method for the obtained powders with subsequent annealing at the temperature 923 K. The values of the ionic and electron components of the total electrical conductivity were obtained analyzing the corresponding frequency dependences of the total electrical conductivity on the Nyquist plots using electrode equivalent circuits. It has been ascertained that reduction of crystallite sizes in Ag_6PS_5I-based ceramic materials leads to a slight increase in ionic conductivity and a significant increase in the electronic one, resulting in a decrease of the ratio between them.

Keywords: argyrodite, superionic conductor, ceramics, impedance spectroscopy, electrical conductivity.

https://doi.org/10.15407/spqeo25.03.294
PACS 82.45.Xy, 91.60.Ed

Manuscript received 23.01.22; revised version received 03.08.22; accepted for publication 21.09.22; published online 06.10.22.

1. Introduction

In recent years, research has been carried out on the transition from traditional Li^+ ion batteries to All-Solid-State Batteries (ASSBs), in which the liquid electrolyte is replaced with a solid-state ionic conductor. Solid-state electrolytes have a number of advantages, they are non-flammable, have a less reactivity to air and battery electrodes [1–5]. Application of solid-state electrolytes not only increases the safety of batteries, but also helps to increase their manufacturability. Therefore, studies of ceramic materials as solid-state electrolytes for their application in batteries are actively performed [6–9]. Widespread commercial application of ASSBs is limited to the search for suitable materials with high values of ionic conductivity in the solid state at room temperature. Among the promising compounds, the representatives of argyrodites – complex ternary or quaternary chalcogenides and chalcohalogenides – are highly attractive. Argyrodites always contain two cations (Me^+ and E^{n+}, where n = 3…5) and are united by a similar structural motif are worth mentioning [10, 11]. The structural motif of argyrodites is a close packing of tetrahedra based on a multicharged cation E^{n+} (rigid anionic sublattice), in the voids of which there are single-charged cations Me^+ with different coordination (linear, trigonal, tetrahedral) [10–12]. Along with different coordination, single-charged cations have different site occupancy factor of crystallographic positions, which defines its disorder. Simultaneous coexistence of the rigid anionic framework and disordered cationic sublattice ensures the mobility of Me^+ ions and relates the argyrodites to superionic conductors [12–15].

The ternary and quaternary argyrodites based on four and five valence elements E^{n+} are the most studied ones. They are characterized by a variety set of properties: optical [16–18], superionic [19–23] and thermoelectric [24, 25]. However, among various argyrodites Ag^+-containing phases with relatively high ionic conductivity in the solid state and high chemical resistance, as compared to the Li^+-containing compounds [26–30], should be mentioned. Ag_6PS_5I crystallizes in the cubic crystal system $F\bar{4}3m$ (No 216) and lattice parameters: a = 10.4745 Å, Z = 4 [30]. Studies of the electrical conductivity of Ag_6PS_5I in the polycrystalline form (obtained using the solid-state synthesis) [26] and monocrystalline samples (crystallization from solution-melt) [30] indicate a high solid-state conductivity. The total electrical conductivity of Ag_6PS_5I obtained in

polycrystalline form is $1.2 \cdot 10^{-4}$S/cm (300 K), and for monocrystalline samples the ionic and electronic conductivity components constitute $1.79 \cdot 10^{-3}$ and $1.64 \cdot 10^{-6}$ S/cm (298 K), respectively. As reported in [18], optical absorption edge of Ag_6PS_5I crystals has an exponential shape and the optical pseudogap is 2.138 eV [18].

This paper is aimed at ascertaining the influence of the recrystallization process on the change of electrical properties of Ag_6PS_5I-based ceramics prepared from micro- and nanocrystalline powders of different dispersion.

2. Experimental

Synthesis of Ag_6PS_5I was carried out from stoichiometric amounts of elemental silver (99.995%), phosphorus (99.99%), sulfur (99.999%), and pre-synthesized binary AgI, additionally purified using the directional crystallization method, in evacuated silica ampoules (0.13 Pa). The synthesis regime included a stepped heating up to 723 K at the rate close to 100 K/h (exposure during 48 h), a further temperature increase up to 1100 K at the rate 50 K/h and ageing at this temperature for 24 hours. The cooling to room temperature was performed in the oven off mode.

Micro- and nanocrystalline powders obtained by grinding in agate mortar and planetary ball mill PQ-N04 at the speed 200 rpm for 30 and 60 min, respectively, were used for preparation of Ag_6PS_5I ceramics. To ensure the appropriate granulometric composition, powders obtained by grinding in an agate mortar were sifted through a sieve with the pore size close to 20 μm. Ag_6PS_5I powders obtained by grinding were studied using powder XRD (AXRD Benchtop, Ni-filtered CuKα radiation, Bragg–Brentano geometry, θ/2θ mode, 2θ scanning angle range 10…90° with dynamic region of interest and exposure 1 s) and SEM technique (powders obtained using grinding in planetary ball mill PQ-N04).

Our analysis of experimental powder patterns (Fig. 1) indicates that powders obtained by grinding in a ball mill are characterized by a significant broadening of the peaks in comparison with microcrystalline powder Ag_6PS_5I, which is a characteristic of nanoscale objects. Also, the appearance of new reflexes and displacement of already existing ones on the powder patterns of samples ground in a planetary ball mill (Fig. 1) is not observed. This indicates that long-term grinding does not cause a change in the crystal structure and degradation of nanopowders. The results of optical microscopy studies (METAM-R1) showed that the sizes of crystallites obtained by grinding in an agate mortar are within ~10…20 μm. Unfortunately, the average size of crystallites in the powder could not be ascertained with a sufficient accuracy, which is caused by its low reflective ability. The analysis of SEM images showed that the average size of crystallites obtained by grinding in a ball mill is indicative of sizes close to ~150 nm (30 min) and ~100 nm (60 min), respectively, which can be seen from the corresponding histograms of particle size distribution (Fig. 2).

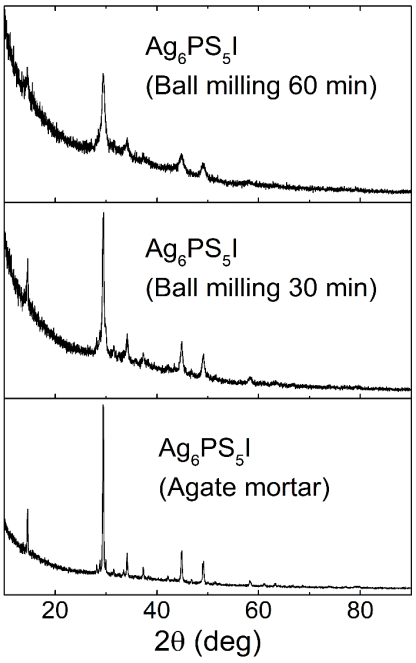

Fig. 1. XRD patterns of micro- and nanocrystalline Ag_6PS_5I powders.

The disks with a diameter of 10 mm and a thickness of 2...3 mm were prepared by cold pressing of the corresponding micro- and nanocrystalline powders at the pressure close to 400 MPa. Ag_6PS_5I-based ceramics was obtained by the annealing of these disks at 923 K for 36 h (heating / cooling rate 20 K/h). The corresponding temperature is ~60 K lower than all thermal effects on the Ag_6PS_5I DTA curve [30]. This should maximally promote the recrystallization process [31], and not just the solid-state annealing of powders. Recrystallization should contribute to increasing the efficiency of ion transport by reducing the number of intercrystalline boundaries, it will also lead to an increase in the mechanical stability of the obtained ceramic materials [32, 33].

It was ascertained using the hydrostatic weighing method that the relative density of disks (before annealing) pressed from microcrystalline powders constitutes 91 ± 1%, while in the case of nanocrystalline powders its value is 94 ± 1% of the theoretical one. It is noteworthy that the recrystallization did not cause an increase/decrease in the porosity of ceramics, as evidenced by similar values of density, which were determined in the materials after annealing.

The prepared ceramic materials were investigated using the microstructural analysis with the metallographic microscope METAM-R1 (Fig. 3) in order to determine the size of crystallites after annealing. According to the results of microstructural analysis, particle size distribution histograms for different time of grinding were plotted (Fig. 3). It was ascertained that ceramic samples obtained by sintering the nanocrystalline powders are characterized by a more homogeneous microstructure characterized by the distribution

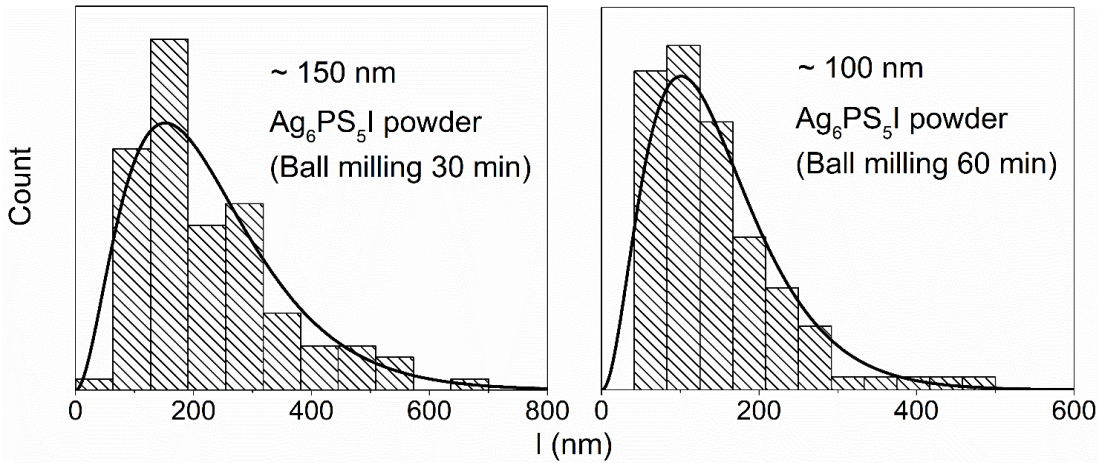

Fig. 2. Histograms of particle size distribution for Ag_6PS_5I powders obtained by grinding in the planetary ball mill.

of particles in a narrower range, in contrast to the samples obtained by sintering the microcrystalline powder with the particle sizes of 10…20 μm. As a result of recrystallization process, the average size of crystallites for ceramics obtained from microcrystalline powder is ~8.2 μm, and from nanocrystalline powders obtained by grinding for 30 and 60 min is ~5.6 and ~3.3 μm, respectively.

The electrical conductivity studies of Ag_6PS_5I-based ceramic materials were performed using impedance spectroscopy [34], within the frequency ($1\cdot10^1$…$3\cdot10^5$ Hz) and temperature (293…383K) ranges with the high-precision LCR meter AT 2818. The amplitude of alternating current was equal to 10 mV. Measurements were carried out using the two-electrode method with blocking (electron) gold contacts. Gold contacts for measurements were applied by chemical precipitation from solutions (293 K) [20, 21]. The analysis of obtained dependences by using the Nyquist plots was performed with the ZView 3.5 program.

3. Results and discussion

The frequency dependences of the total electrical conductivity for Ag_6PS_5I-based ceramic materials (Fig. 4) are typical, which is manifested in the increase of electrical conductivity with frequency. This is one of the characteristic features, which indicates the presence of ionic conduction. However, it should be noted that the above-mentioned growth is insignificant, *i.e.*, occurs only within one order, which is obviously caused by the relatively high values of electron component of the electrical conductivity.

It was found that the decrease in size of crystallites 8.2 → 5.6 → 3.3 μm (insert to Fig. 4) causes a slight increase in the total electrical conductivity that is determined at the frequency 100 kHz. For a detailed analysis of frequency behavior inherent to the total electrical conductivity in order to determine the contributions of ionic and electron conduction, a standard approach using electrode equivalent circuits (EEC) [34–36] was used.

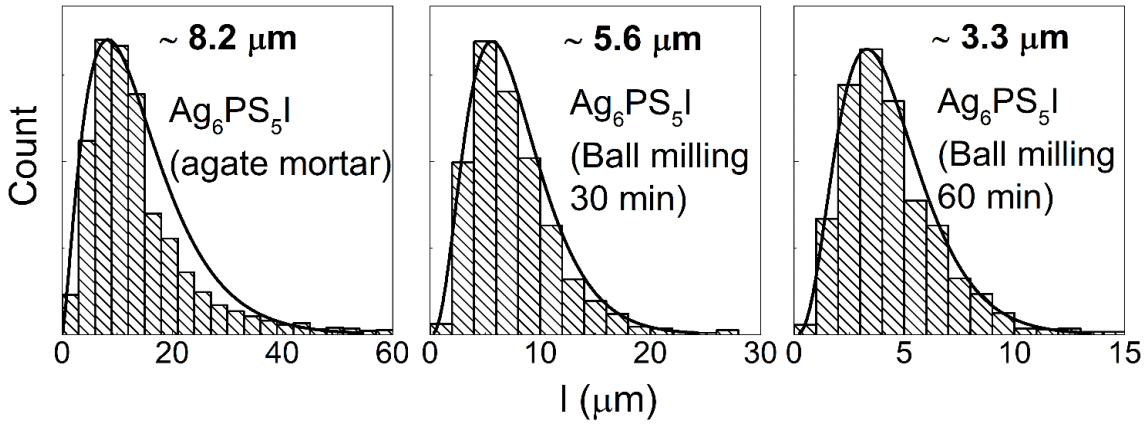

Fig. 3. Histograms of crystallite size distribution for Ag_6PS_5I ceramic samples obtained by sintering the micro- and nanocrystalline powders.

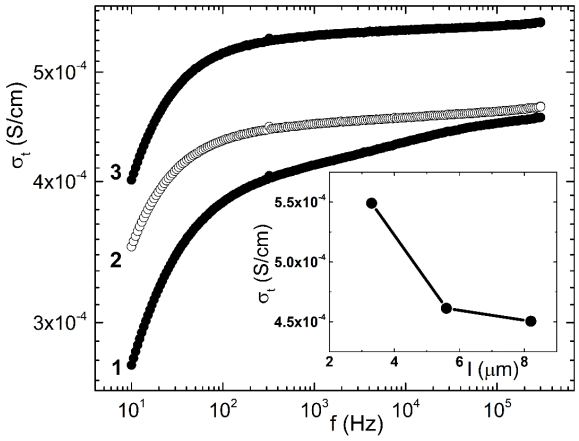

Fig. 4. Frequency dependences of the total electrical conductivity for Ag_6PS_5I-based ceramic materials: *1* – 8.2, *2* – 5.6, *3* – 3.3 μm. The insert shows the dependence of total electrical conductivity (f = 100 kHz) on the size of crystallites (T = 298 K).

This includes analysis of frequency dependences on Nyquist plots. The parasitic inductance of the cell (~$2\cdot10^{-8}$ H) is taken into account during this analysis.

Ceramics made of micro- and nanocrystalline Ag_6PS_5I powders are characterized by a mixed ionic-electronic type of electrical conduction, like to that of single crystals of the corresponding composition [30]. For all ceramic materials, two semicircles (Fig. 5) within the temperature range ~293…353 K are observed, except for ceramics with a crystallite size of 8.2 μm (Fig. 5a, curve *1*), for which three semicircles are observed. Frequency behavior of electrical conductivity for all the ceramics could be explained using single EEC (Fig. 5). For low-frequency semicircles in the Nyquist plots, the capacitance of double diffusion layer C_{dl} with sequentially included parameters R_{gb}/C_{gb} (resistance and capacitance of grain boundaries) is responsible. These parameters, in turn, are responsible for the end of the low-frequency semicircle, and in the case of ceramics with the crystallite size 8.2 μm (Fig. 5a, curve *1*) cause the appearance of a medium-frequency semicircle. The appearance of the latter (Fig. 5a, curve *1*) can be explained by clearer grain boundaries formed during the annealing of microcrystalline powders and a wider range of crystallite distribution in contrast to that in ceramics pressed from nanocrystalline powders (Fig. 3).

For high-frequency semicircles (Fig. 5, curves *1* and *2*) in the Nyquist plots of all cases, the resistance and capacitance of intracrystalline boundaries (R_{db}/C_{db}) are responsible, which can be considered low-angle domains. Their formation is most likely facilitated by sintering the crystallites with different crystallographic orientation.

Above 353 K, all these materials are characterized by the presence of only one semicircle in the Nyquist plots (Fig. 5, curve *3*). In this case, the above parameters responsible for the resistance and capacitance of grain and intracrystalline boundaries represent the high-frequency section of the semicircle. The degeneracy of two semicircles into one is primarily associated with the growth of the electronic component of electrical conductivity.

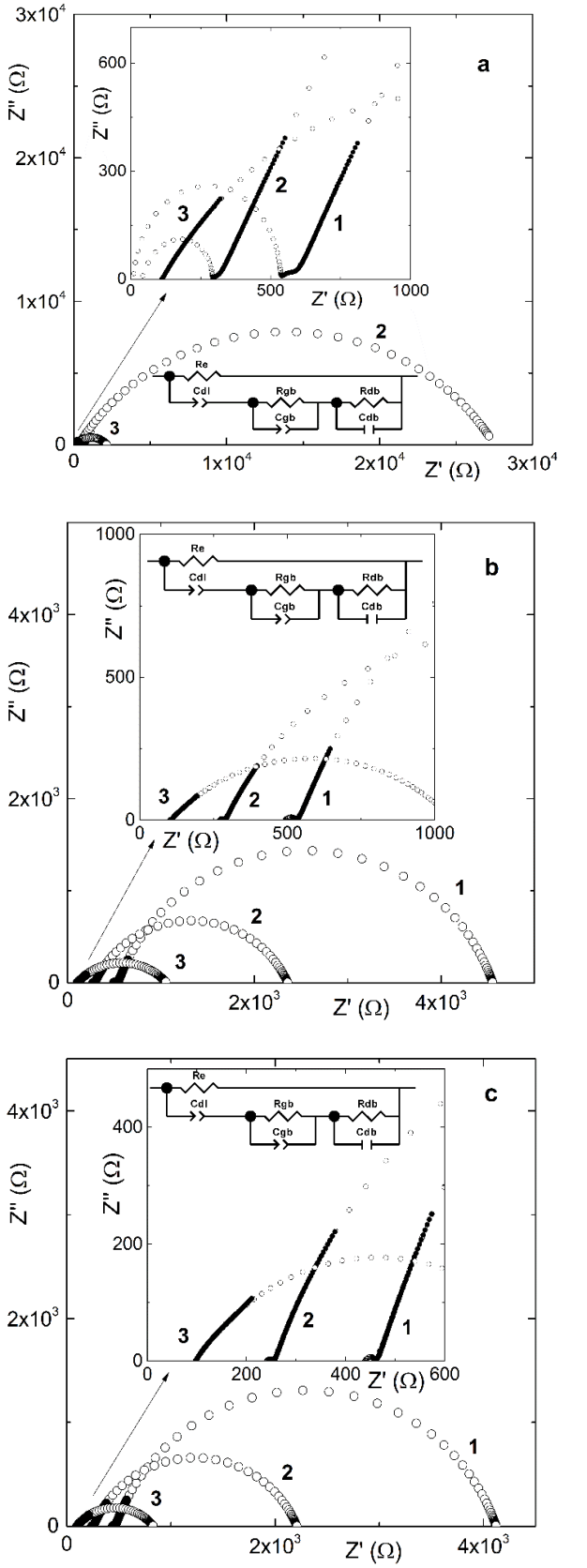

Fig. 5. EEC and Nyquist plots for Ag_6PS_5I-based ceramics with different dispersion: (a) 8.2 μm, (b) 5.6 μm, (c) 3.3 μm; *1* – 298 K, *2* – 323 K, *3* – 373 K. Experimental data are designated with the filled circles, and the calculated ones – with the blank circles.

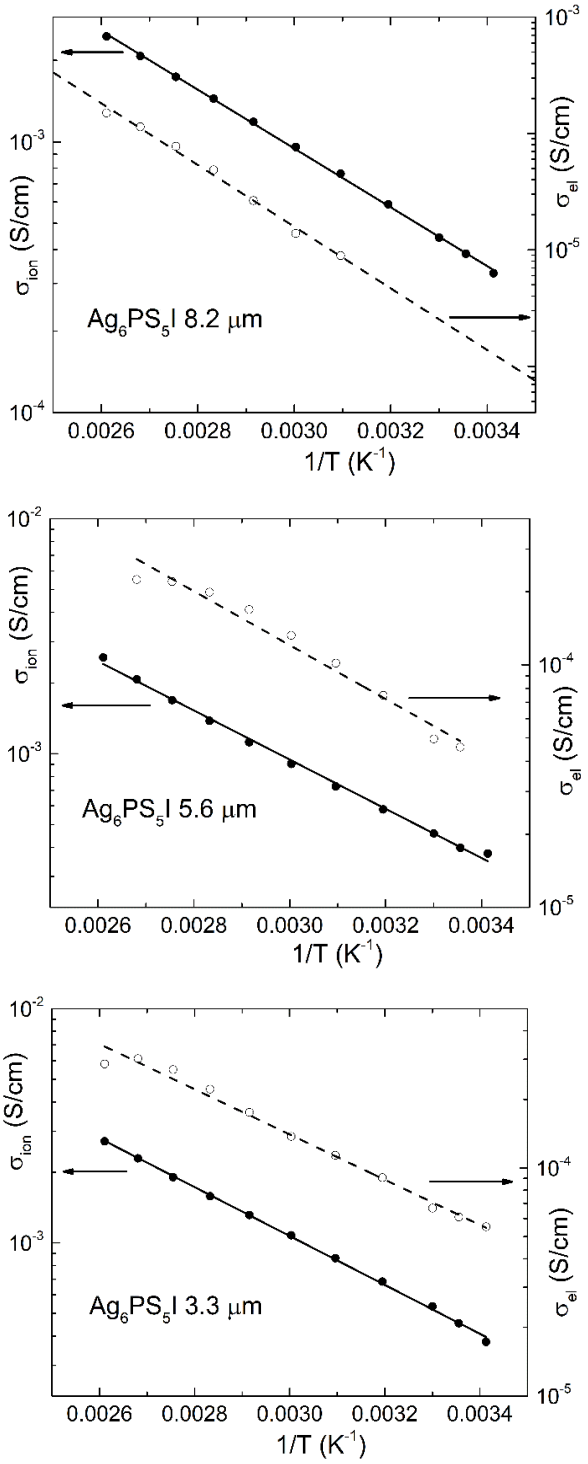

Fig. 6. Temperature dependences of ionic and electronic components of electrical conductivity for Ag_6PS_5I-based ceramics.

Thus, the ionic component of electrical conductivity is determined by the sum of the resistances responsible for the grain and intracrystalline boundaries of ceramic materials. In parallel with the above-described ionic processes, the electronic resistance R_e, which is responsible for the electronic component of electrical conductivity, was introduced into EEC.

The performed analysis of impedance spectra made it possible to study the temperature dependence of components of electrical conductivity and to ascertain the influence of size effect on the change in ionic and electronic conductivity. The temperature dependences of the electronic and ionic components of electrical conductivity in the Arrhenius coordinates are shown in Fig. 6. It was found that for all the ceramic materials made on the basis of Ag_6PS_5I they are linear, which indicates the thermal activation nature of electrical conductivity. This provided an opportunity to calculate the activation energies of both components providing the electrical conductivity.

It was ascertained that the decrease in the size of crystallites 8.2 → 5.6 → 3.3 μm (Fig. 7a) leads to a monotonous increase in the values of both ionic and electronic components of electrical conductivity, and if the value of ionic conductivity increases within $3.86\cdot10^{-4}…4.54\cdot10^{-4}$S/cm, the value of the electronic component increases by more than an order of magnitude. It results in a monotonous decrease in the ratio between the components of electrical conductivity (insert to Fig. 7a).

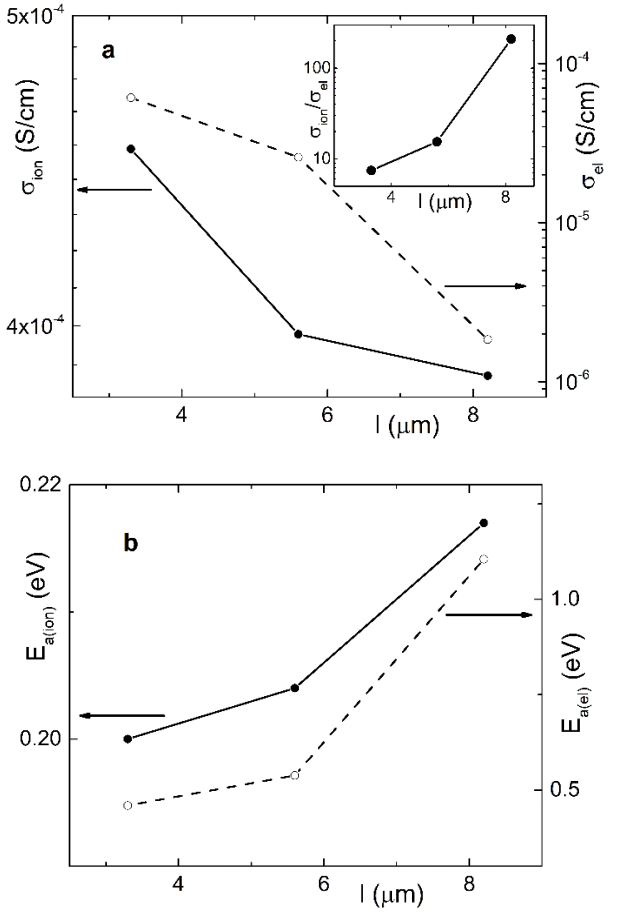

Fig. 7. Dependence of ionic, electronic conductivity (a) (T = 298 K) and their activation energies (b) on the dispersion of Ag_6PS_5I-based ceramic material. The insert shows the ratio between the components of electrical conduction (T = 298 K).

Fig. 7b shows the dependence of the activation energy of the ionic and electronic components of electrical conduction on the size of the crystallites. There is a monotonous decrease in the activation energies of both components inherent to the electrical conduction. This behavior of electrical conduction components and their activation energies can be partially associated with a decrease in porosity by $3 \pm 1\%$ (for ceramics with the crystallite sizes of 8.2 → 5.6 μm), which, as described above, was determined by the hydrostatic weighing. However, further reduction in the crystallite sizes of Ag_6PS_5I ceramic to 3.3 μm does not lead to a change in porosity, while the values of electrical conduction components continue to increase, and their activation energies decrease (Fig. 7). Probably, the main factor is the different recrystallization ability of micro- and nanocrystalline powders. Namely, the sintering of larger size (~10…20 μm) crystallites can cause a less degree of recrystallization, as compared to nanocrystalline powders with an average crystallite size of ~150 and ~100 nm. This can result a tendency that the decrease in a crystallites size of initial powders will lead to a decrease in the number of distinct intercrystallite boundaries and, accordingly, cause the increase of "blurred" boundaries. Undoubtedly, reducing the number of boundaries with a distinct surface separation will contribute to the increase in the values of both components of electrical conduction and the reduction of their activation energies.

4. Conclusions

Superionic conductor Ag_6PS_5I was synthesized from the melt and further was grinded to a micro- and nanocrystalline powders. XRD studies showed that the grinded Ag_6PS_5I powders aren't prone to degradation. For grinded in ball mill powders, a significant broadening of the diffraction peaks was observed, which is typical for nanoscale objects. The Ag_6PS_5I-based superionic ceramics in the form of disks with the diameter 10 mm and thickness 2...4 mm were obtained using the solid-state sintering method of microcrystalline and nanocrystalline powders.

Using the optical microscopy method, it was established that the size of the crystallites after sintering of different size powders stay within the range of 8.2 to 3.3 μm. Using the impedance spectroscopy method, the measurement of total electrical conductivity was carried out within the temperature 293…383 K and frequency $1 \cdot 10^1 \ldots 3 \cdot 10^5$ Hz ranges on the corresponding ceramic materials. It has been ascertained that the decrease in crystallite sizes 8.2 → 5.6 → 3.3 μm causes a slight increase in the total electrical conductivity. The electrical conduction was further separated into ionic and electronic components by analyzing the Nyquist plots by using EEC. It has been ascertained that prepared Ag_6PS_5I ceramics are characterized by a mixed ion-electronic type of electrical conduction.

It was ascertained that a decrease in the crystallite sizes (8.2 → 3.3 μm) of ceramics corresponds to a certain increase in the values of both the ionic and electronic components of electrical conduction. The increase in the values of the electronic component of electrical conduction is more significant than that of the ionic component. This leads to a decrease in the ratio between the components of electrical conduction. It has been ascertained that the temperature dependences of the electrical conductivity components are subject to the Arrhenius equation, which allowed us to determine the corresponding activation energies for all ceramic materials. A decrease in the values of corresponding activation energies for both components of electrical conduction has been observed. This behavior of components of electrical conduction and their activation energy can be related to the increase in the number of intercrystalline boundaries ("blurred") during the recrystallization of different dispersion powders.

References

1. Yu C., Zhao F., Luo J., Zhang L., Sun X. Recent development of lithium argyrodite solid-state electrolytes for solid-state batteries: Synthesis, structure, stability and dynamics. *Nano Energy*. 2021. **83**. P. 105858. https://doi.org/10.1016/j.nanoen.2021.105858.
2. Wu J., Liu S., Han F., Yao X. Wang C. Lithium/sulfide all-solid-state batteries using sulfide electrolytes. *Adv. Mater*. 2021. **33**. P. 2000751. https://doi.org/10.1002/adma.202000751.
3. Wang C., Liang J., Zhao Y. *et al.* All-solid-state lithium batteries enabled by sulfide electrolytes: from fundamental research to practical engineering design. *Energy Environ. Sci.* 2021. **14**. P. 2577–2619. https://doi.org/10.1039/D1EE00551K.
4. Sun C., Liu J., Gong Y., Wilkinson D.P., Zhang J. Recent advances in all-solid-state rechargeable lithium batteries. *Nano Energy*. 2017. **33**. P. 363–386. https://doi.org/10.1016/j.nanoen.2017.01.028.
5. Randau S., Weber D.A., Kötz O. *et al.* Benchmarking the performance of all-solid-state lithium batteries. *Nat. Energy*. 2020. **5**. P. 259–270. https://doi.org/10.1038/s41560-020-0565-1
6. Zhu J., Li X., Wu C. *et al.* A multilayer ceramic electrolyte for all-solid-state Li batteries. *Angew. Chem. Int. Ed.* 2021. **60**. P. 3781–3790. https://doi.org/10.1002/anie.202014265.
7. Zhou L., Minafra N., Zeier W.G., Nazar L.F. Innovative approaches to Li-argyrodite solid electrolytes for all-solid-state lithium batteries. *Acc. Chem. Res.* 2021. **54**. P. 2717–2728. https://doi.org/10.1021/acs.accounts.0c00874.
8. Shen Y., Zhang Y., Han S. *et al.* Unlocking the energy capabilities of lithium metal electrode with solid-state electrolytes. *Joule*. 2018. **2**. P. 1674–1689. https://doi.org/10.1016/j.joule.2018.06.021.
9. Wang S., Tang M., Zhang Q. *et al.* Lithium argyroditeas solid electrolyte and cathode precursor for solid-state batteries with long cycle life. *Adv. Energy Mater*. 2021. **11**. 2101370. https://doi.org/10.1002/aenm.202101370.

10. Kuhs W.F., Nitsche R., Scheunemann K. The argyrodites – a new family of tetrahedrally close-packed structures. *Mat. Res. Bull*. 1979. **14**. P. 241–248. https://doi.org/10.1016/0025-5408(79)90125-9.
11. Nilges T., Pfitzner A. A structural differentiation of quaternary copper argyrodites: Structure–property relations of high temperature ion conductors. *Z. Kristallogr*. 2005. **220**. P. 281–294. https://doi.org/10.1524/zkri.220.2.281.59142.
12. Morgan B.J. Mechanistic origin of superionic lithium diffusion in anion-disordered Li_6PS_5X argyrodites. *Chem. Mater*. 2021. **33**. P. 2004–2018. https://doi.org/10.1021/acs.chemmater.0c03738.
13. Hanghofer I., Brinek M., Eisbacher S.L. *et al*. Substitutional disorder: structure and ion dynamics of the argyrodites Li_6PS_5Cl, Li_6PS_5Br and Li_6PS_5I. *Phys. Chem. Chem. Phys*. 2019. **21**. P. 8489–8507. https://doi.org/10.1039/C9CP00664H.
14. Adeli P., Bazak J.D., Park K.H. *et al*. Boosting solid-state diffusivity and conductivity in lithium superionic argyrodites by halide substitution. *Angew. Chem. Int. Ed*. 2019. **58**. P. 8681–8686. https://doi.org/10.1002/anie.201814222.
15. Zhang Z., Sun Y., Duan X. *et al*. Design and synthesis of room temperature stable Li-argyrodite superionic conductors *via* cation doping. *J. Mater. Chem. A*. 2019. **7**. P. 2717–2722. https://doi.org/10.1039/C8TA10790D.
16. Semkiv I., Ilchuk H., Pawlowski M., Kusnezh V. Ag_8SnSe_6 argyrodite synthesis and optical properties. *Opto-Electron. Rev*. 2017. **25**. P. 37–40. https://doi.org/10.1016/j.opelre.2017.04.002.
17. Studenyak I.P., Izai V.Yu., Studenyak V.I. *et al*. Interrelations between structural and optical properties of $(Cu_{1-x}Ag_x)_7GeS_5I$ mixed crystals. *Ukr. J. Phys. Opt*. 2018. **19**. P. 237–243. https://doi.org/10.3116/16091833/19/4/237/2018.
18. Studenyak I.P., Pop M.M., Shender I.O., Pogodin A.I., Kranjcec M. Temperature behaviour of fundamental absorption edge in superionic Ag_6PS_5I crystals. *Ukr. J. Phys. Opt*. 2021. **22**. P. 216–224. https://doi.org/10.3116/16091833/22/4/216/2021.
19. Pogodin A.I., Filep M.J., Malakhovska T.O. *et al*. The copper argyrodites $Cu_{7-n}PS_{6-n}Br_n$: Crystal growth, structures and ionic conductivity. *Solid State Ionics*. 2019. **341**. P. 115023. https://doi.org/10.1016/j.ssi.2019.115023
20. Studenyak I.P., Pogodin A.I., Studenyak V.I. *et al*. Electrical properties of copper- and silver-containing superionic $(Cu_{1-x}Ag_x)_7SiS_5I$ mixed crystals with argyrodite structure. *Solid State Ionics*. 2020. 345. P. 115183. https://doi.org/10.1016/j.ssi.2019.115183.
21. Studenyak I.P., Pogodin A.I., Filep M.J. *et al*. Influence of heterovalent cationic substitution on electrical properties of $Ag_{6+x}(P_{1-x}Ge_x)S_5I$ solid solutions. *J. Alloys Compd*. 2021. **873**. P. 159784. https://doi.org/10.1016/j.jallcom.2021.159784.
22. Kraft M.A., Ohno S., Zinkevich T. *et al*. Inducing high ionic conductivity in the lithium superionic argyrodites $Li_{6+x}P_{1-x}Ge_xS_5I$ for all-solid-state batteries. *J. Am. Chem. Soc*. 2018. **140**. P. 16330−16339. https://doi.org/10.1021/jacs.8b10282.
23. Chen H.M., Maohua C., Adams S. Stability and ionic mobility in argyrodite-related lithium-ion solid electrolytes. *Phys. Chem. Chem. Phys*. 2015. **17**, No 25. P. 16494−16506. http://doi.org/10.1039/C5CP01841B.
24. Lin S., Li W., Pei Y. Thermally insulative thermoelectric argyrodites. *Mater. Today*. 2021. **48**. P. 198−213. https://doi.org/10.1016/j.mattod.2021.01.007.
25. Studenyak I.P., Pogodin A.I., Luchynets M.M. *et al*. Influence of heterovalent substitution on structural, electrical and thermoelectric properties of $Cu_{7-x}PS_{6-x}Br_x$ solid solutions. *J. Phys. Chem. Solids*. 2021. **150**. P. 109855. https://doi.org/10.1016/j.jpcs.2020.109855.
26. Beeken R.B., Garbe J.J., Gillis J.M. *et al.* Electrical conductivities of the Ag_6PS_5X and the Cu_6PSe_5X (X=Br, I) argyrodites. *J. Phys. Chem. Solids.* 2005. **66**. P. 882−886. https://doi.org/10.1016/j.jpcs.2004.10.010.
27. Beeken R.B., Garbe J.J., Petersen N.R., Stoneman M.R. Electrical properties of the Ag_6PSe_5X (X=Cl, Br, I) argyrodites. *J. Phys. Chem. Solids*. 2004. **65**. P. 1011−1014. https://doi.org/10.1016/j.jpcs.2003.10.060.
28. Laqibi M., Cros B., Peytavin S., Ribes M. New silver superionic conductors Ag_7XY_5Z (X = Si, Ge, Sn; Y = S, Se; Z = Cl, Br, I)-synthesis and electrical studies. *Solid State Ionics*. 1987. **23**. P. 21−26. https://doi.org/10.1016/0167-2738(87)90077-4.
29. Beeken R.B., Driessen C.R., Hinaus B.M., Pawlisch D.E. Electrical conductivity of Ag_7PSe_6 and Cu_7PSe_6. *Solid State Ionics*. 2008. **179**. P. 1058−1060. https://doi.org/10.1016/j.ssi.2008.01.014.
30. Studenyak I.P., Pogodin A.I., Filep M.J. *et al*. Crystal structure and electrical properties of Ag_6PS_5I single crystal. *SPQEO*. 2021. **24**. P. 26−33. https://doi.org/10.15407/spqeo24.01.026.
31. Rollett A., Rohrer G.S., Humphreys J. *Recrystallization and Related Annealing Phenomena*. Elsevier. 2017.
32. Cheikh A., Madani A., Touati A. *et al*. Ionic conductivity of zirconia based ceramics from single crystals to nanostructured polycrystals. *J. Eur. Ceram. Soc.* 2001. **21**. P. 1837−1841. https://doi.org/10.1016/S0955-2219(01)00126-1.
33. Šalkus T., Kazakevičius E., Banys J. *et al*. Influence of grain size effect on electrical properties of Cu_6PS_5I superionic ceramics. *Solid State Ionics*. 2014. **262**. P. 597−600. https://doi.org/10.1016/j.ssi.2013.10.040.
34. Orazem M.E., Tribollet B. *Electrochemical Impedance Spectroscopy*. New Jersey: John Wiley & Sons, 2008. https://doi.org/10.1002/9780470381588.
35. Barsoukov E., Macdonald J.R. *Impedance Spectroscopy: Theory, Experiment, and Applications*. Hoboken, New Jersey: John Wiley & Sons. 2018. https://doi.org/10.1002/9781119381860.

36. Huggins R.A. Simple method to determine electronic and ionic components of the conductivity in mixed conductors a review. *Ionics*. 2002. **8**, No 3. P. 300−313. https://doi.org/10.1007/BF02376083.

Authors and CV

Artem I. Pogodin, defended his PhD thesis in inorganic chemistry in 2016. Senior researcher at the Uzhhorod National University. Authored over 53 articles and 90 patents. The area of his scientific interests includes solid state chemistry, crystal growth, and materials science.
https://orcid.org/0000-0002-2430-3220

Iryna O. Shender, born in 1995. Currently she is PhD student at the Uzhhorod National University, Faculty of Physics. Authored of 8 articles and 4 patents. The area of scientific interests is electrical and optical properties of superionic conductors.
E-mail: shender95@gmail.com,
https://orcid.org/0000-0003-1687-3634

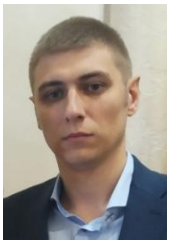

Mykhailo J. Filep, born in 1987, defended his PhD thesis in inorganic chemistry in 2015. Senior researcher at the Uzhhorod National University. Authored over 40 articles and 20 patents. The area of his scientific interests includes solid state chemistry and materials science.
E-mail: mfilep23@gmail.com,
http://orcid.org/0000-0001-7017-5437

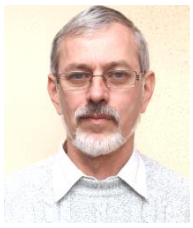

Oleksandr P. Kokhan, PhD, Associate professor of Inorganic Chemistry department, Uzhhorod National University. Authored over 80 articles and 95 patents. The area of his interests includes inorganic chemistry, solid state chemistry, crystal growth, materials science.
E-mail: aleksandr.kokh@gmail.com,
http://orcid.org/0000-0003-1534-6779

Tetyana O. Malakhovska, born in 1983, defended her PhD thesis in inorganic chemistry in 2010. Senior researcher at the Uzhhorod National University. Authored 45 articles and 10 patents. The area of her scientific interests includes solid state chemistry and materials science.
E-mail: t.malakhovska@gmail.com,
https://orcid.org/0000-0001-7309-4894

Olesya I. Simkanych, born in 1986. In 2016 she defended her PhD thesis in the specialty 21.06.01 – environmental safety. Currently, he is an associate professor of the Department of Ecology and Environmental Protection of the Uzhhorod National University. Author of 32 articles and 4 patents. Research interests: chemistry, chemical and radioecological monitoring, drug standardization, GIS in ecology.
E-mail: olesjasi123@gmail.com,
https://orcid.org/0000-0002-9948-1742

Leonid M. Suslikov, Doctor of Physical and Mathematical Sciences, Professor, Department of Applied Physics at the Uzhhorod National University. Authored over 200 articles, 22 patents, 2 monograph, 42 textbooks. The area of his scientific interests includes solid state physics, optical properties of complex semiconductor compounds, frequency and spatial dispersion of optical constants in disordered systems.
E-mail: leonsus48@gmail.com,
https://orcid.org/0000-0003-4628-5972.

Peter Kopčanský, PhD, Research Professor in condensed matter physics. Leading scientist of Institute of Experimental Physics, Slovak Academy of Sciences. Authored over 300 articles, 10 patents, 1 monograph, 10 chapters in books. The area of his scientific interests includes solid state physics, especially magnetism, transport properties in disordered magnetic systems, magnetic fluids, their magnetic and dielectric properties, composite systems with liquid crystals and technical as well as biomedical applications of magnetic nanoparticles.
E-mail: kopcan@saske.sk,
https://orcid.org/ 0000-0002-5278-9504

Authors' contributions

Pogodin A.I.: supervision, conceptualization, investigation, writing – original draft.
Shender I.O.: investigation, visualization.
Filep M.J.: investigation, writing – original draft.
Kokhan O.P.: methodology, writing – review & editing.
Symkanych O.I.: investigation.
Malakhovska T.O.: investigation, writing – original draft.
Suslikov L.M.: writing – review & editing.
Kopčanský P.: methodology, writing – review & editing.

Вплив розмірів кристалітів на електричні властивості керамічних матеріалів на основі Ag_6PS_5I

А.І. Погодін, І.О. Шендер, М.Й. Філеп,О.П. Кохан, О.І. Симканич, Т.О. Малаховська, Л.М. Сусліков, П. Копчанський

Анотація. Шляхом розмелювання попередньо синтезованого Ag_6PS_5I в агатовій ступці та планетарному кульовому млині одержано мікро- та нанокристалічні порошки, які в подальшому досліджено з використанням методів XRD та SEM. Методом холодного пресування одержаних порошків з подальшим відпалом при температурі 923 K виготовлено відповідні керамічні матеріали у формі дисків з густиною (91…94) ± 1% від теоретичної. Значення іонної та електронної складових загальної електропровідності одержано шляхом аналізу відповідних частотних залежностей загальної електропровідності на діаграмах Найквіста з використанням еквівалентних схем електродів. Установлено, що зменшення розмірів кристалітів керамічних матеріалів, виготовлених на основі Ag_6PS_5I, приводить до незначного зростання іонної складової та суттєвого зростання електронної складової провідності, що викликає зменшення співвідношення між ними.

Ключові слова: аргіродит, суперіонний провідник, кераміка, імпедансна спектроскопія, електропровідність.